Modeling of an Industrial Fluidized-Bed Granulator for Urea Production

Diego E. Bertin,[†] Germán D. Mazza,[‡] Juliana Piña,[†] and Verónica Bucalá*,[†]

Department of Chemical Engineering, PLAPIQUI, Universidad Nacional del Sur, CONICET, Camino La Carrindaga Km. 7, (8000) Bahía Blanca, Argentina, and Department of Chemistry, Faculty of Engineering, Universidad Nacional del Comahue, Buenos Aires 1400, (8300) Neuquén, Argentina

The steady−state operation of a continuous industrial fluidized-bed granulator for urea production with multiple growth and cooling beds in series is modeled. The model is based on mass and energy balances, which account for the behavior of all the phases that coexist within the unit, as well as the bed hydrodynamics patterns. The granules growth that occurs through the deposition of droplets on urea seeds, followed by water evaporation and solidification of the urea present in the solution, is taken into account by considering the concentrated nature of the inlet urea solution. The proposed mathematical model successfully predicts industrial data for different plant capacities. The total urea dissolution heat is the most important thermal effect involved in the growth chambers. The granulator operation provides significant heat and mass transfer within the unit, with the water evaporation being almost complete and the outlet gas and particle temperatures being very similar.

1. Introduction

Particle size enlargement techniques are used in every industrial process that handles particulate feeds, intermediates or products.[1] Granulation converts fine powders and/or sprayed liquids (e.g., suspensions, solutions or melts) to granular solids. A wide variety of industries utilize granulation to produce particles with defined properties to meet specific end-use requirements (among others, mining, food processing, pharmaceuticals, and fertilizer manufacture).[2] The advantages of a fluidized bed, with respect to other granulation systems, include the coupling of spraying, granulation, drying, and cooling stages in one single unit and control, within certain limits, of the granules physical properties by manipulation of some operating variables.[3]

Fertilizers have an essential role in securing food supplies around the world. Their importance to the survival of the human race should not be underestimated. There is no way the entire world can be properly fed without the extensive use of fertilizers.[4] The world population has doubled over the period from 1960 to 2000, and it is currently increasing at a rate of 90 million people per year.[5] Fertilizers are produced in either liquid or granular form. The bulk production of fertilizers is mainly in granular form, which has the advantage of possessing excellent storage, handling, and transport properties.[4] Within commercial fertilizers, those based on nitrogen are used most often; more than 40% of the world dietary protein is currently derived from nitrogen fertilizers.[5] Among all nitrogen-based fertilizers, urea is the most widely produced. Urea consumption is increasing significantly, because of its nitrogen content and flexibility to be combined with other types of fertilizers.[6]

Fluidized-bed granulation for urea production was successfully implemented on an industrial scale at Sluiskil in 1979 by NSM Sluiskil (then Hydro Agri, later Yara, and, today, Uhde). This process became the leading technology, with more than 50 reference plants possessing single-stream capacities with a range of 500−3600 mt/d. Currently, there are urea plants based on fluidized-bed granulation on all five continents, and new capacities are constantly being added.[7]

Despite the widespread use and large-scale application of this process in the fertilizers industry and the significant advances in understanding the fundamentals of granulation during the last two decades, to the best of our knowledge, there is a lack of work that involved the modeling and simulation of continuous urea industrial fluidized-bed granulators. A thorough understanding and detailed representation of the fluidized-bed hydrodynamics and the mechanisms prevailing in the process are important and essential to estimate a priori granule characteristics, such as size and moisture, from a knowledge of the operating conditions and the physical and chemical properties of the seeds and fertilizer solution.[8,9] Currently, considerable trial and error is required to obtain the fluidized-bed granulator operating parameters that would allow stable operations and granules production with the desired attributes. Such tuning is highly dependent on the operator's experience.[10,11]

The urea fluidized-bed granulator is basically a bed of solids fluidized by air, fed continuously with small urea particles (seeds) and a urea concentrated liquid solution (∼96%[12,13]) that is sprayed from the bottom of the unit. The bubbling nature of the fluidized bed, which is responsible for the strong solids mixing, promotes the repeatedly circulation of the granules through the spraying zone. The granules grow through the deposition of tiny liquid droplets on the seed material, followed by cooling and evaporation of the water content of the droplets, which cause the solidification of the urea present in the solution. The energy for the evaporation is provided by the urea solution itself, which is atomized into the granulator at a relatively high temperature (∼413 K[12,13]). To increase the residence time of the granules, some industrial units possess three growth chambers (where the urea concentrated solution is sprayed) connected by regulating flaps. Subsequently, fluidized bed dedusting/cooling compartments are arranged to meet specific requirements for further processing of the granules.

Physically based mathematical models, with different degrees of complexity, have been presented in the open literature for the heat- and mass-transfer processes in liquid-sprayed fluidized

* To whom correspondence should be addressed. Tel: 54-291-486-1700, ext. 265. Fax: 54-291-486-1600. E-mail address: vbucala@plapiqui.edu.ar.

[†] Department of Chemical Engineering, PLAPIQUI, Universidad Nacional del Sur, CONICET.

[‡] Department of Chemistry, Faculty of Engineering, Universidad Nacional del Comahue.

10.1021/ie070361o CCC: $37.00
Published on Web 08/10/2007

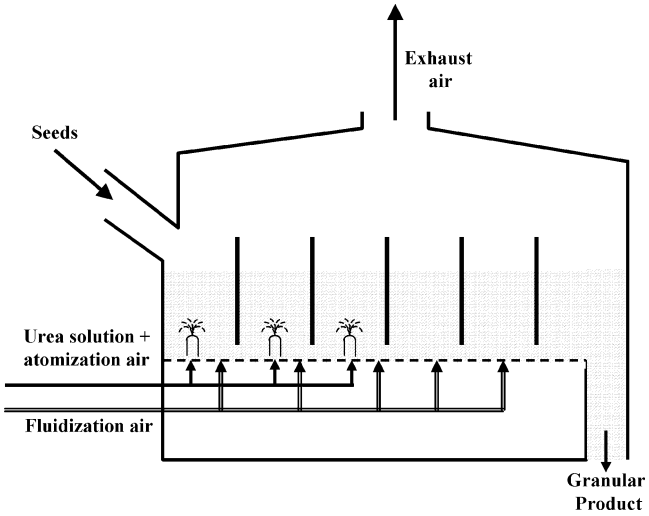

Figure 1. Simplified schematic representation of an industrial fluidized-bed granulator for urea production.

beds used for granulation.[14−16] These models not only describe the temperature and concentration distributions in fluidized-bed spray granulators, but also the wetting and deposition of the sprayed-in droplets onto the fluidized-bed particles. While the governing equations of the process and the numerical solution have been thoroughly documented, the models have been evaluated with experimental data from pilot-scale units using ideal materials such as glass beads sprayed with pure water.[14−16]

In this work, the steady-state operation of a continuous industrial fluidized-bed granulator for urea production is simulated as growth and cooling chambers in series by means of a detailed mathematical model. The mass and heat exchanges between the different compartments are considered. The model for each granulation chamber is based on the mass and energy balances for the three phases (urea solid particles, urea concentrated liquid solution, and atomization and fluidization humid air) that coexist within the unit. The hydrodynamics and mass exchange between the different regions (bubbles and emulsion phases) of the fluidized gas are taken into account. Particular emphasis is put on the definition of the driving force that governs the evaporation of the water content of the liquid droplets. Special attention is given to the concentrated nature of the urea solution (i.e., urea solubility and heat of dissolution), which affect the water composition of the sprayed droplets in the granulator as well as the overall heat balance. The simulation results are compared with data from an industrial urea plant.

2. Mathematical Model

Figure 1 shows a schematic representation of an industrial continuous fluidized bed for urea granulation.[6] The unit has multiple internal chambers divided by weirs; the first three chambers are used for urea granulation, while the others are reserved for dedusting and, to some extent, product cooling. A concentrated urea solution (usually called urea melt) is bottom-sprayed, using atomization air, in the granulation chambers. The fluidization air inlet casing is the lower part of the unit. This processing gas enters to the granulator through a gas distributor. Each chamber can handle different fluidization air flow rates and temperatures.[17] Solid particles are continuously fed to the first chamber of the granulator. The seeds are constituted by recycled crushed oversized particles and undersized granules. The fluidized particles undercurrent flows through the unit in a horizontal direction, toward the granulator outlet. The mass and energy balances for the industrial granulator are formulated,

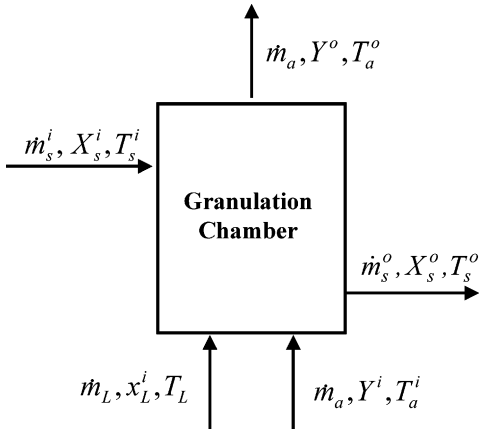

Figure 2. Scheme of a granulation chamber showing the main streams, water compositions, and temperatures.

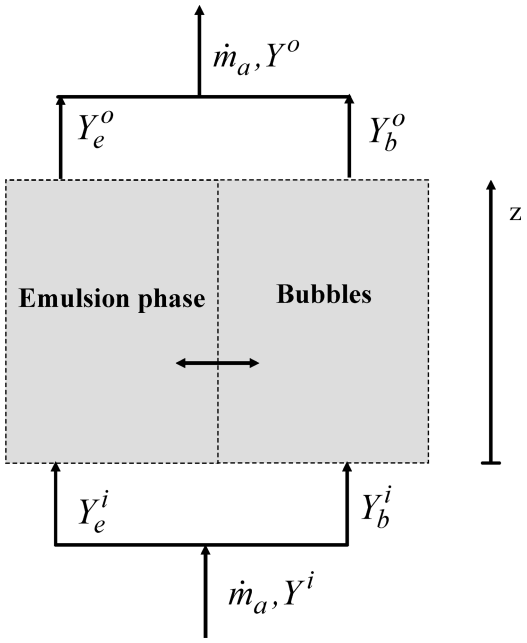

Figure 3. Two-phase bubbling bed theory.

including the mass and heat exchanges between chambers. However, to introduce the mathematical model clearly, the modeling of an isolated granulation chamber is first presented and discussed.

2.1. Mathematical Model of an Isolated Granulation Chamber. The fluidized-bed urea granulator is represented by a heterogeneous model, where three phases are considered: solid (urea particles), liquid (urea melt), and gas (humid air). Figure 2 shows the main streams and the nomenclature used to denote flow rates, water compositions, and temperatures of the granulation chamber. The two-phase theory, which was first introduced by Toomey and Johnstone,[18] is used to describe the structure of the bubbling fluidized bed as schematized in Figure 3. The emulsion (dense phase) is constituted by solid particles, urea solution droplets, and air under minimum fluidization conditions, whereas the excess gas circulates through the bed as bubbles. According to the Geldart classification of particles,[19] urea granules belong to Group D. Therefore, the superficial gas velocity in the dense phase (u_e) will reach higher values than the bubble superficial velocity (u_b). Under this condition, according to Davidson's theory, the gas uses the bubble as a convenient shortcut on its way through the bed and no cloud is expected.[20] In the model formulation, bubbles then rise slowly and no clouds need to be considered.

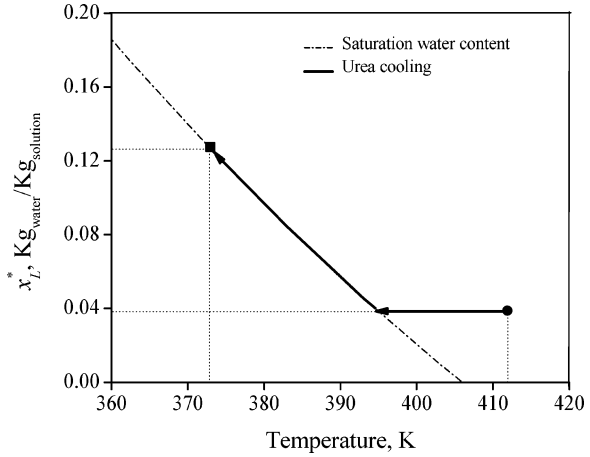

Figure 4. Water contents of saturated urea solutions, as a function of temperature.

The following hypothesis are assumed for the model formulation:

(1) The granulation chamber operates at steady-state conditions.

(2) The solid and liquid phases are perfectly mixed.

(3) Plug flow is assumed for the gas that circulates in the emulsion phase.

(4) The gas in the bubbles is assumed to be perfectly mixed; the bubbles rise as plug flow.

(5) The presence of solids inside the bubbles is neglected, according to Fitzgerald's considerations for the coarse particle fluidization regime.[21]

(6) The urea granules have constant density and are spherical. The urea granules are supposed to be free of additives such as formaldehyde.

(7) The elutriation of fines, and the formation of nuclei by attrition, breakage, and/or overspray are neglected. In fact, all the urea melt droplets are assumed to reach the surface of the seeds. Based on industrial experimental evidence, the agglomeration of particles is also disregarded.

(8) The seeds and product particles are characterized by the corresponding median diameter.

(9) The water evaporation occurs at the droplet/emulsion gas interface; when the water vapor reaches the emulsion phase, it may be transported to the bubbles.

(10) The mass-transfer area for water evaporation is the total surface area of the particles. Because liquid loading allows the formation of many layers onto the particles within the bed, complete wetting is considered.

(11) The moisture gradients inside the granules and droplets are neglected.

2.1.1. Mass Balances: Solid and Liquid Phases. 2.1.1.1. Urea. The solid mass growth can be expressed as

$$\dot{m}_S^0 = \dot{m}_S^i + \dot{m}_L(1 - x_L^i) \tag{1}$$

2.1.1.2. Water. The water content of the granular product is mainly a function of the water loading and the water that is evaporated in the fluidized bed:

$$X_S^\circ = \frac{\dot{m}_S^i X_S^i + \dot{m}_L x_L^i - \dot{m}_{ev}}{\dot{m}_S^\circ} \tag{2}$$

2.1.2. Mass Balances: Gas Phases. 2.1.2.1. Water (Emulsion). The water that is evaporated from the droplets deposited onto the particles surface is first transported to the interstitial gas (emulsion phase), and from there to the bubbles. The mass balance for the water in the air at the emulsion phase becomes

$$\frac{dY_e}{dz} = \frac{\beta_{PE}}{D_p}(Y^* - Y_e) - \left(\frac{\delta}{\epsilon - \delta}\right)\left(\frac{\beta_{EB}}{D_b}\right)(Y_e - Y_b) \tag{3}$$

where

$$\beta_{PE} = \frac{6k_{PE}\rho_a A_T \epsilon(1 - \epsilon_{mf})}{\dot{m}_a \epsilon_{mf}} \tag{4}$$

$$\beta_{EB} = \frac{6k_{EB}\rho_a A_T \epsilon}{\dot{m}_a} \tag{5}$$

The first term on the right-hand side of eq 3 is related to the evaporation of water from the droplets to the emulsion gas, whereas the second term represents the mass transport between the emulsion phase and the bubbles. The mass-transfer coefficients k_{PE} and k_{EB} are calculated according to the guidelines given by Kunii and Levenspiel.[22]

2.1.2.2. Water (Bubbles).

$$\frac{dY_b}{dz} = \frac{\beta_{EB}}{D_b}(Y_e - Y_b) \tag{6}$$

The moisture content of the total air along the axial coordinate can be computed as follows:

$$Y = \left(\frac{\epsilon_{mf}(1 - \delta)}{\epsilon}\right)Y_e + \left(\frac{\delta}{\epsilon}\right)Y_b \tag{7}$$

The boundary conditions to solve eqs 3 and 6 are

$$z = 0 \tag{8a}$$

$$Y_e^i = Y_b^i = Y^i \tag{8b}$$

The total evaporated water flow rate can be calculated as a function of the inlet and outlet air humidities through eq 9:

$$\dot{m}_{EV} = \dot{m}_a(Y^o - Y^i) \tag{9}$$

2.1.3. Outlet Diameter. Assuming a constant number particle flow, the median diameter of the granules at the exit of the granulation chamber is computed using the following equation:

$$D_p^o = D_p^i\left[\frac{\dot{m}_S^o(1 + X_S^o)}{\dot{m}_S^i(1 + X_S^i)}\right]^{1/3} \tag{10}$$

Usually, the moisture content of the granules is not considered to contribute to the granule volume. In fact, the water contents of the seeds and granular product in industrial urea granulators are very low; therefore, it is commonly assumed that $X_s^o = X_s^i \approx 0$.[23]

2.1.4. Hydrodynamics. Several properties related to the hydrodynamics of the fluidized bed must be evaluated to define the system completely. Table 1 presents the correlations and expressions used in the present work. The variables and correlations associated to the minimum fluidization conditions were computed based on the Chitester et al. work.[24] The expressions to evaluate the bubbles diameter correspond to those reported by Mori and Wen.[25] The air velocities and porosities were calculated following the guidelines given by Kunii and Levenspiel.[22]

Table 1. Fluidynamics Properties

property	notation	correlation/value
superficial gas velocity under minimum fluidizing conditions	u_{mf}	$\frac{Re_{mf}\,\mu}{\rho_a D_p}$
particle Reynolds number under minimum fluidizing conditions	Re_{mf}	$\sqrt{28.7^2 + 0.0494Ar} - 28.7$
porosity under minimum fluidizing conditions	ϵ_{mf}	0.41
superficial total velocity	u	$\frac{\dot{m}_a(1+Y)}{A_T\rho_a}$
terminal velocity	u_t	$\frac{\left(\frac{\mu(\rho_S-\rho_a)g}{\rho_a^2}\right)^{1/3}}{\frac{18}{Ar^{1/3}}+\frac{2.335-1.744}{Ar^{1/3}}}$
bubbles		
diameter above the distributor	D_{b_0}	$\frac{1.30}{g^{0.2}}\left[\frac{u-u_{mf}}{N_{or}}\right]^{0.4}$
equilibrium size	D_b^*	$2.59g^{-0.2}[A_T(u-u_{mf})]^{0.4}$
size	D_b	$D_b^* - (D_b^* - D_{b0})\exp\left[-\frac{0.3z}{\sqrt{4A_T/\pi}}\right]$
relative velocity	u_{b_r}	$0.711\sqrt{g\overline{D}_b}$
velocity	u_b	$u - u_{mf} + u_{br}$
emulsion gas velocity	u_e	u_{mf}/ϵ_{mf}
bubble fraction in the fluidized bed	δ	$\frac{u-u_{mf}}{u_b - qu_{mf}}$ $u_b < u_e \quad q = 2$ $u_e < u_b < 2.5u_e \quad q = 1$ $2.5u_e < u_b < 5u_e \quad q = 0$ $u_b > 5u_e \quad q = -1$
total bed porosity	ϵ	$\delta + \epsilon_{mf}(1-\delta)$

2.1.5. Water Evaporation. 2.1.5.1. Equilibrium Moisture. The equilibrium moisture involved in eq 3 can be calculated using the modified Raoult's law:

$$y^* = \gamma \frac{x_L}{M_w\left[\frac{1}{M_u}(1-x_L)+\frac{1}{M_w}x_L\right]}\left(\frac{P^V}{P}\right) \qquad (11)$$

where x_L represents the water content of the melt droplets within the granulation chamber. To derive the right representation of this composition, urea solubility concepts are introduced. The solubility of a solid solute can be calculated as a function of temperature, according to[26]

$$\ln S = -\frac{\Delta H_{FUS}}{R}\left(\frac{T_{FUS}-T}{T\,T_{FUS}}\right) \qquad (12)$$

where S, which is expressed in units of $kmol_{urea}/kmol_{solution}$, represents the maximum urea content that the solution is permitted to have. Therefore, the water content of a saturated solution is given by

$$x_L^* = \frac{1-S}{1+S\left(\frac{M_u}{M_w}-1\right)} \qquad (13)$$

Figure 4 shows the x_L^* values (calculated by means of eqs 12 and 13), as a function of temperature. The predicted values are in good agreement with experimental solubilities.[6] The selected temperature range covers the industrial operating temperatures (an inlet urea melt temperature of ~413 K and fluidized-bed temperatures in the range of 363−383 K[12,13]). Typically, the urea melt is sprayed into the system at ~413 K and has preferably ~0.4 wt % water;[12,13] this inlet operating point is referenced in Figure 4 with a solid circle. Because the urea droplets are very small (20−120 μm),[27] a very rapid decrease of the droplet temperature down to the fluidized-bed temperature is assumed. If the heat transfer is much faster than the water mass transport, the water content of the droplets should suffer a rapid increase to its saturation value (see the solid square symbol in Figure 4). Although evaporation occurs within the granulator chamber, the water concentration of the droplets should remain constant and equal to the equilibrium x_L^* value until complete drying is achieved. The x_L^* value can be calculated after the fluidized-bed temperature is defined, and this is the variable that should be used to compute the water equilibrium concentration (y^*) in the emulsion gas at the droplet/emulsion interface (see eq 11). The activity coefficient (γ) was determined to be close to 0.9 for the studied operating conditions. Thus, for modeling purposes, the nonideality of the solution is neglected and Raoult's law is used to evaluate y^*.

2.1.5.2. Evaporation Rate Modeling. The water evaporation in urea granulators is not commonly limited by the mass transport at the droplet/emulsion-gas interface, mainly because (a) the amount of water in the urea melt is very low to saturate the air stream that circulates through the bed, (b) the temperature level is high enough to reinforce the trend toward water evaporation, and (c) the relatively high value of the particle−gas mass-transfer rate in urea bubbling fluidized beds (obtained through multiplication of the mass-transfer coefficient by the exposed specific area).[28] Even though the y^* value defined by eq 11 with $x_L = x_L^*$ is used in the driving force of eq 3 (instead of the air saturation humidity that corresponds to $x_L = 1$), the evaporation flow (the first term on the right-hand side of eq 3)

still can be very important. In consequence, the evaporated water flow rate calculated by eq 9 may be higher than the available inlet water flow rate. This problem, which has been recognized by several authors,[14,23,29] occurs because the evaporation term in eq 3 is independent of the water liquid loading. Several works are focused on the evaluation of the degree of wetting, which can be interpreted as a parameter that corrects the mass-transfer area and, thus, the evaporation transfer rate (first term on the right-hand side of eq 3). If axial measurements of the air moisture are not accessible, the accuracy of the models is difficult to be established.[29] The aforementioned difficulty becomes also important for the urea granulation modeling. Another point of view to overcome this problem is presented below.

If eq 3 is multiplied by $\dot{m}_{a\,e}$, which is defined as $\dot{m}_{a\,e} = (\epsilon_{mf}(1-\delta))/(\epsilon)\,\dot{m}_a$, the following expression is obtained:

$$\dot{m}_{a\,e}\frac{dY_e}{dz} = \frac{\beta_{PE}}{D_p}\left(\frac{\epsilon_{mf}(1-\delta)\,\dot{m}_a}{\epsilon}\right)(Y^* - Y_e) - \frac{\delta}{\epsilon-\delta}\left(\frac{\beta_{EB}}{D_b}\right)\left(\frac{\epsilon_{mf}(1-\delta)\,\dot{m}_a}{\epsilon}\right)(Y_e - Y_b) \quad (14)$$

The first term on the right-hand side of eq 14 represents the axial gradient of the evaporation rate; rearrangement of this term gives

$$d\dot{m}_{EV} = \frac{\beta_{PE}}{D_p}\left(\frac{\epsilon_{mf}(1-\delta)\,\dot{m}_a}{\epsilon}\right)(Y^* - Y_e)\,dz = \frac{6k_{PE}\rho_a A_T(1-\epsilon)}{D_p}(Y^* - Y_e)\,dz \quad (15)$$

In addition, at every Δz, the water evaporation flow rate is limited by a maximum water flow rate, which is given by the inlet water flow rate per unit length.[16] Therefore, the following relationship should be satisfied:

$$d\dot{m}_{EV} \le \frac{\dot{m}_L x_L^i}{L}\,dz \quad (16)$$

Inequality 16 can be also expressed as the following equality:

$$\frac{6k_{PE}\rho_a A_T(1-\epsilon)}{D_p}(Y^* - Y_e)\,dz = \xi(z)\frac{\dot{m}_L x_L^i}{L}\,dz \quad (17)$$

where $\xi(z)$ represents the fraction of the available water flow rate that evaporates in Δz; this parameter should verify the following constraints:

$$0 \le \xi(z) \le 1 \quad (18)$$

From eq 17, $\xi(z)$ becomes

$$\xi(z) = \frac{6k_{PE}\rho_a A_T L(1-\epsilon)}{D_p \dot{m}_L x_L^i}[Y^* - Y_e(z)] \quad (19)$$

The minimum possible evaporated fraction $\xi(z)$ would occur at the granulator outlet, because, in that position, the driving force would achieve its lowest value. As a maximum, the outlet humidity in the emulsion air would be

$$Y_e^{max}(L) = Y^i + \frac{\dot{m}_L x_L^i}{\dot{m}_{a\,e}} \quad (20)$$

By replacing eq 20 in eq 19, the following relationship is obtained:

$$\xi(L) = \frac{6k_{PE}\rho_a A_T L(1-\epsilon)}{D_p \dot{m}_L x_L^i}\left[Y^* - \left(Y^i + \frac{\dot{m}_L x_L^i}{\dot{m}_{a\,e}}\right)\right] \quad (21)$$

Equation 21 represents the minimum possible evaporation fraction along the granulator height. If $\xi(L) \ge 1$, the mass transfer between phases (at any axial position) would not control the evaporation process (eq 15 cannot be used to represent the evaporation rate). For the industrial urea granulator studied in the present work, $\xi(L) \gg 1$; therefore, the evaporation rate is limited by the water availability as follows:

$$d\dot{m}_{EV} = \frac{\dot{m}_L x_L^i}{L}\,dz \quad (22)$$

Using eq 22, the mass balance for the emulsion gas becomes

$$\frac{dY_e}{dz} = \frac{\epsilon \dot{m}_L x_L^i}{\epsilon_{mf}(1-\delta)\dot{m}_a L} - \frac{\delta}{\epsilon-\delta}\left(\frac{\beta_{EB}}{D_b}\right)(Y_e - Y_b) \quad (23)$$

2.1.6. Heat Balances. The heat balances for the urea granulator, which is represented by a heterogeneous model, must take into consideration different thermal effects. In addition to the sensible heats associated to the streams that enter and leave the granulator, latent heats are also involved. When the water evaporates from the urea solution, two important thermal phenomena occur. The energy required to sustain the water evaporation comes mainly from the urea melt; this thermal effect contributes to a reduction of the fluidized-bed temperature. However, while the water evaporation occurs, the urea that is dissolved in the urea melt becomes solid. This process releases the heat of dissolution of the urea (which takes into account the fusion and mixing heats), balancing, to some extent, the endothermic heat of evaporation. The heat of evaporation, per mass unit, the urea is ~9 times higher than the heat of dissolution for the urea. Nevertheless, because of the high urea concentration of the solution (~96%), the total heat of dissolution is much higher than the heat of evaporation and, of course, cannot be neglected.

In addition to the model assumptions already described, the following hypotheses are considered:

(1) The temperatures of the liquid and solid phases are equal.

(2) The temperatures of the emulsion gas and bubble phase are the same.

(3) The chamber, *as isolated*, operates adiabatically.

Figure 5 shows the mass and heat flows involved in the heat balances.

2.1.6.1. Solid and Liquid Phases.

$$\dot{m}_S^i \int_{T_S^o}^{T_S^i} cp_{US}\,dT + \dot{m}_S^i X_S^i \int_{T_S^o}^{T_S^i} cp_W\,dT + \dot{m}_L(1-x_L^i)\int_{T_S^o}^{T_L} cp_{US}\,dT + \dot{m}_L x_L^i \int_{T_S^o}^{T_L} cp_W\,dT + \dot{m}_L \Delta H_{DIS}(T_L) - \dot{m}_{EV}\Delta H_{EV}(T_S^o) + \dot{Q}_{APL} = 0 \quad (24)$$

where $\dot{Q}_{APL}$ represents the heat flow exchanged with the air.

2.1.6.2. Gas Phase.

$$\frac{dT_a}{dz} = \frac{\beta_{PE}\alpha}{D_p}(T_S^o - T_a) + \frac{\lambda}{D_p}(T_S^o - T_a) \quad (25)$$

where α and λ are defined as follows:

$$\alpha = \frac{(Y^* - Y)cp_V}{cp_a + Y\,cp_V} \tag{26}$$

$$\lambda = \frac{6hA_T(1-\epsilon)}{\dot{m}_a(cp_a + Y\,cp_V)} \tag{27}$$

The first term on the right-hand side of eq 25 is related to the enthalpy of the evaporated water flow that is incorporated to the gas phase; the second term represents the heat flow exchanged between the air−particle/liquid film interface. The gas−particle heat-transfer coefficient (h) is calculated following the guidelines given by Kunii and Levenspiel.[22]

The boundary condition necessary for eq 25 is given by

$$z = 0 \tag{28a}$$

$$T_a = T_a^i \tag{28b}$$

The $\dot{Q}_{APL}$ heat flow, which is required to solve eq 24, is calculated by averaging the axial heat flow profile as follows:

$$\dot{Q}_{APL} = \int_0^L h\left(\frac{6}{D_p}\right)A_T(1-\epsilon)(T_a - T_S^o)\,dz \tag{29}$$

2.1.6.3. Total Heat Balance. After the outlet temperatures of the air and particles have been computed, the following global heat balance must be verified:

$$\dot{m}_S^i \int_{T_S^o}^{T_S^i} cp_{US}\,dT + \dot{m}_S^i X_S^i \int_{T_S^o}^{T_S^i} cp_W\,dT + \dot{m}_L(1 - x_L^i)\int_{T_S^o}^{T_L} cp_{US}\,dT + \dot{m}_L x_L^i \int_{T_S^o}^{T_L} cp_W\,dT + \dot{m}_a \int_{T_a^o}^{T_a^i} cp_a\,dT + \dot{m}_a Y^i \int_{T_a^o}^{T_a^i} cp_V\,dT + \dot{m}_L \Delta H_{DIS}(T_L) - \dot{m}_{EV}\Delta H_{EV}(T_S^o) = 0 \tag{30}$$

2.2. Mathematical Model of an Industrial Granulator with Multiple Chambers. To model multiple fluidized beds in series, the mass and heat flows between chambers must be considered. The mass balances described for an isolated chamber can be directly applied to the growth cells. For the cooling chambers, the urea solution is not fed, and, therefore, $\dot{m}_L$ should to be set equal to zero. The isolated chamber heat balances must be corrected to account for the rate of heat flow exchanged with the surroundings and contiguous fluidized beds (see Figure 6); i.e., the hypothesis of adiabatic chambers is now removed. For this general case, the gas energy balance becomes

$$\frac{dT_{aj}}{dz} = \frac{\beta_{PE}\alpha + \lambda}{D_p}(T_{Sj}^o - T_{aj}) + \frac{U_{j(j-1)}A_{j(j-1)}}{\dot{m}_a(cp_a + Y\,cp_V)}(T_{a(j-1)} - T_{aj}) + \frac{U_{j(j+1)}A_{j(j+1)}}{\dot{m}_a(cp_a + Y\,cp_V)}[T_{a(j+1)} - T_{aj}] + \frac{U_{jext}A_{jext}}{\dot{m}_a(cp_a + Y\,cp_V)}(T_{ext} - T_{aj}) \tag{31}$$

For the first growth cell, the parameter $A_{j(j-1)}$ is zero, whereas, for the last cooling chamber, $A_{j(j+1)}$ becomes null. To calculate the overall heat-transfer coefficient between fluidized beds, the heat conduction through the weir is neglected and the following general expression is applied:

$$\frac{1}{U_{jk}} = \frac{1}{\hat{h}_j} + \frac{1}{\hat{h}_k} \tag{32}$$

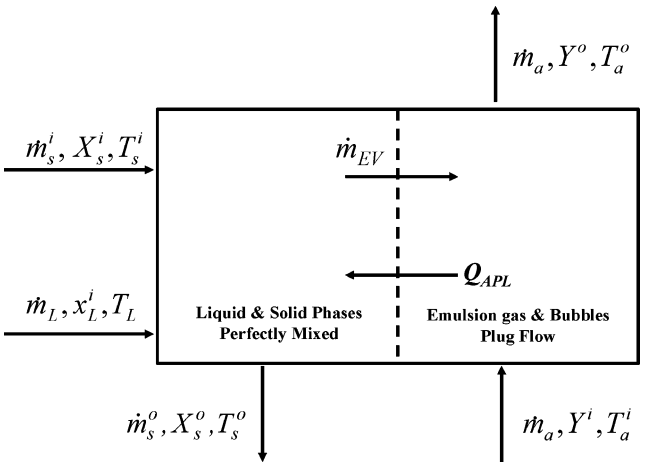

Figure 5. Mass and heat flows involved in the heat balances, for an adiabatic chamber.

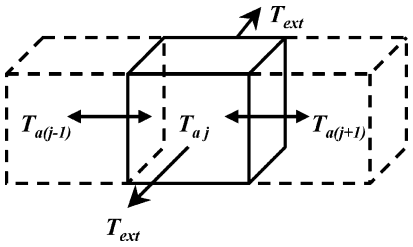

Figure 6. Heat exchange between the chambers and the surroundings.

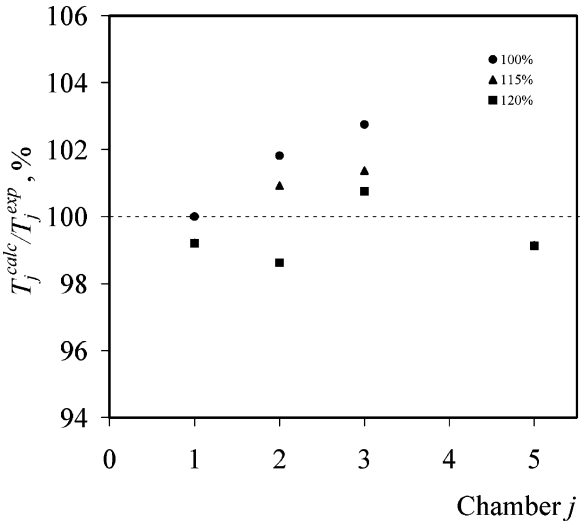

Figure 7. Ratio between the calculated and experimental bed temperatures for all the granulation chambers and the last cooling compartment, for different plant capacities.

The heat-transfer coefficient $\hat{h}$ between the fluidized bed and the wall is evaluated from

$$\hat{h} = h_e(1 - \delta_{wall}) + h_b\delta_{wall} \tag{33}$$

where δ_{wall} is the volumetric average bubble fraction near the wall, and h_e and h_b are the emulsion and bubble phase contributions to the global heat-transfer coefficient, respectively. The h_e component and volume fraction of bubbles in vicinity of the wall (δ_{wall}) are evaluated with the expressions derived by Mazza et al.[30] The correlation proposed by Mazza et al.[31] is used to determine the value of the bubble phase component (h_b).

To calculate the overall heat-transfer coefficient between the fluidized-bed chamber and the surroundings, an expression

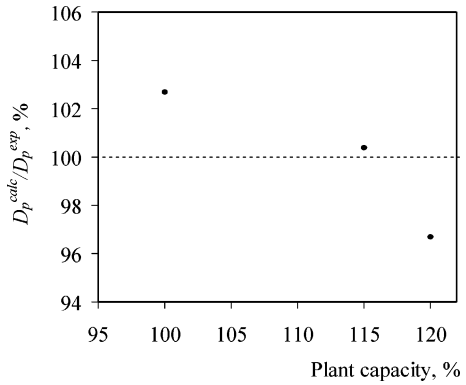

Figure 8. Ratio between the calculated and experimental outlet median particle diameters for different plant capacities.

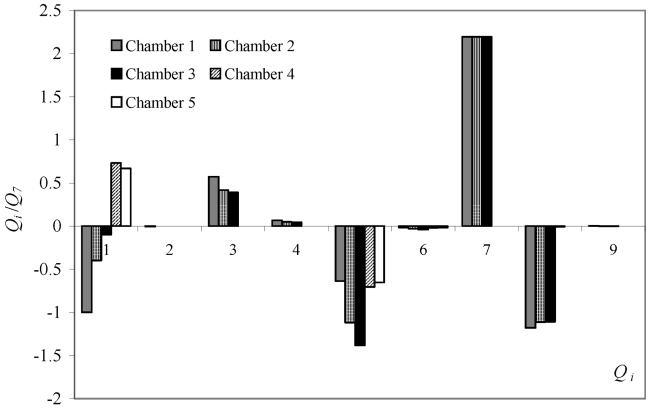

$$Q_1 \quad m_S^i \int_{T_S^o}^{T_S^i} cp_{US}\, dT \qquad Q_5 \quad m_a \int_{T_a^o}^{T_a^i} cp_a\, dT$$

$$Q_2 \quad m_S^i\, X_S^i \int_{T_S^o}^{T_S^i} cp_W\, dT \qquad Q_6 \quad m_a Y^i \int_{T_a^o}^{T_a^i} cp_V\, dT$$

$$Q_3 \quad m_L \left(1 - x_L^i\right) \int_{T_S^o}^{T_L} cp_{US}\, dT \qquad Q_7 \quad m_L\, \Delta H_{DIS}\left(T_L\right)$$

$$Q_4 \quad m_L\, x_L^i \int_{T_S^o}^{T_L} cp_W\, dT \qquad Q_8 \quad -m_{EV}\, \Delta H_{EV}\left(T_S^o\right)$$

Q_9 *Heat exchange with the neighbor chambers and the surroundings.*

Figure 9. Relative heat flows involved in the global heat balance (eq 22, including the exchange of heat with the surroundings and contiguous beds) for the granulation and cooling chambers.

similar to eq 32 is used:

$$\frac{1}{U_{j\,\mathrm{ext}}} = \frac{1}{\hat{h}_j} + \frac{1}{h_{\mathrm{ext}}} \tag{34}$$

A natural convection correlation is applied to evaluate h_{ext}.[32]

Regarding the particle/liquid-phase energy balance, eq 24 is also used when multiple chambers are modeled. The particle contribution to the heat-transfer coefficient between the emulsion and chamber wall (h_e) is not dominant under the studied operating conditions and particle diameters. Then, the convective component of the interstitial gas in the emulsion is the effect that controls the value of this coefficient. In consequence, it is reasonable to establish that the heat is transferred from particles to gas and that this gas phase is the responsible for the heat that is transported toward the chamber walls.

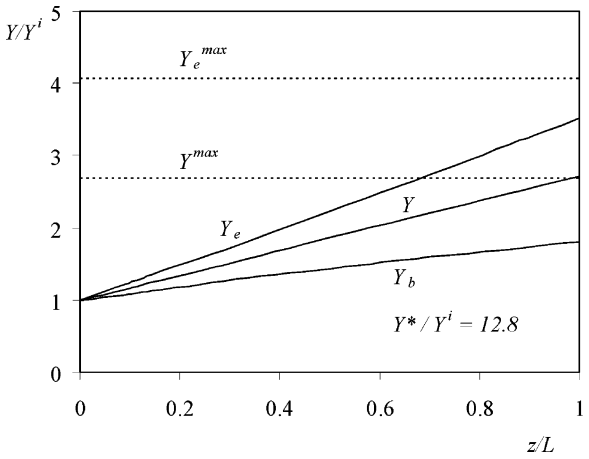

Figure 10. Air humidity axial profiles for the emulsion gas and bubbles. Plant capacity: 115%, first chamber.

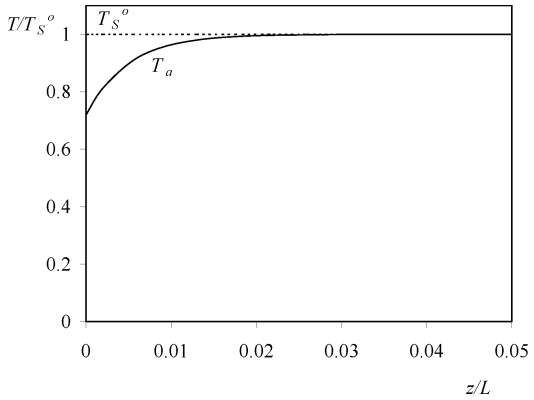

Figure 11. Air temperature axial profile and outlet granules temperature. Plant capacity: 115%, first chamber.

2.3. Urea Physical Properties. Table 2 summarizes all the urea physical properties used in the present work. The water and air properties required for the granulation unit modeling are available in many sources.[26,32,31]

3. Results and Discussion

The presented mathematical model has been validated with experimental data from a continuous industrial fluidized-bed granulator for urea production. The industrial data were obtained for three different plant capacities (100%, 115%, and 120%). The bed temperatures of the granulator chambers were monitored every 15 min, over a period of 15 h under stable operating conditions (i.e., without any change in the operating variables). Samples of the seeds and granular product were collected and analyzed granulometrically every 4 h. As an example of the accuracy of the model predictions, Figure 7 shows, for all the granulation chambers and the last cooling compartment, the ratio between the calculated and experimental outlet bed temperatures, corresponding to the three studied plant capacities. According to the simulation results (see Figure 11), the solid particles and gas phase leave the granulator chamber at almost the same temperature. Therefore, a single temperature value can be used to represent the thermal level of each fluidized bed. The temperatures estimated by the proposed model, which does not include any adjustable parameter, are in very good agreement with the industrial data. In fact, the maximum deviations are <3%.

For the studied operating conditions, Figure 8 presents the ratio between the calculated and experimental outlet median

Table 2. Urea Physical Properties

property	notation	equation/value	units	parameter range	source
urea density	ρ_s	1333.8	kg/m^3		ref 33
density of urea aqueous solution	ρ_L	$1226.40 - 90.61x_L^2 - 124.61x_L$	kg/m^3	$x_L = 0-0.6$	ref 34
heat capacity					
solid urea	$\hat{c}p_{US}$	$17.250 + 0.2318T + 0.000079T^2$	kJ/(kmol K)	$T = 80-400$ K	ref 33
liquid urea	$\hat{c}p_{UL}$	120.5	kJ/(kmol K)	$T = 406$ K	ref 33
fusion temperature	T_{FUS}	406	K		ref 34
heat of fusion	$\Delta\hat{H}_{FUS}$	15060	kJ/kmol	$T = 406$ K	ref 34
heat of dissolution	$\Delta\hat{H}_{DIS}$	14580	kJ/kmol	$T = 406$ K	ref 34
heat of mixing	$\Delta\hat{H}_{MIX}$	-480	kJ/kmol	$T = 406$ K	ref 34
activity coefficient	γ	$\ln\gamma = \Delta H_{MIX}/(RT)$			ref 26

particle diameters, as a function of the plant capacity. The predicted granule diameter, which is computed from the experimental median diameter of the seeds size distribution and the particle growth rate that results from the solution of the urea mass balance (eq 10), well-reproduces the size grade number (i.e., median diameter) of the experimental product size distribution.

The moisture measured in the product was extremely low, indicating that the total evaporation flow rate was almost equal to the water liquid loading. Regretfully, further details of the industrial information must remain proprietary.

The proposed model allows not only the evaluation of the temperatures, flow rates, and composition of all the outlet streams, but also evaluation of some other interesting information, as the importance of the thermal effects of the different phenomena that take place within the granulator. Figure 9 illustrates, for the granulation and cooling chambers, the magnitude of the various terms that constitute the global heat balance (eq 22, considering the heat exchange with the surroundings and contiguous beds), with respect to the total heat dissolution term. As mentioned previously, the heat term related to the urea dissolution cannot be neglected; actually, it constitutes the highest energy source in the granulation compartments. The total evaporation heat does not balance that released by the urea dissolution. As expected, only the terms associated with the sensible heat of the particles and air streams are significant in the cooling chambers. According to the magnitude of the term that represents the exchange of heat with the surroundings and contiguous compartments, all the beds operate almost adiabatically.

Figure 10 shows the humidity axial profiles of the emulsion gas and bubble phase for the first growth chamber and a 115% plant capacity. For both gas phases, the air humidity increases almost linearly in the axial direction. The mass-transport resistance between the emulsion and bubbles phases is not negligible; i.e., the moisture content of the emulsion phase is much higher than that which corresponds to the air in the bubbles. The humidity of the total fluidization air (Y) that leaves the growth bed ($z = L$) is very similar to the maximum moisture level defined by the water liquid loading ($Y^{max} = Y^i + \dot{m}_L x_L^i/\dot{m}_a$). This result is in good agreement with the almost-null water granule content found experimentally. The exhaust air is far from the equilibrium humidity value (Y^*).

As illustrated in Figure 11, for the first growth chamber and a plant capacity of 115%, the air temperature increases strongly, up to its outlet value over a short distance from the gas distributor. The temperature of the solid particles that leave the bed is almost identical to the average air temperature. Therefore, it is proved that, from a thermal point of view, the heterogeneous nature of the urea granulation bed can be neglected without losing accuracy in the representation of the system.

4. Conclusions

A detailed mathematical model for the steady-state operation of a multibed fluidized urea granulator has been described and validated against industrial data without using any adjustable parameter. In this work, aspects related to the use of concentrated liquid solutions, as the urea melt, are introduced for the purpose of providing modeling tools which are not limited to applications where very diluted solutions are considered. The heat of the urea dissolution is a key variable for the overall heat balance. For those systems that use molten fertilizers (i.e., without water) as atomizable liquids, other thermal effects that are associated with fusion and/or phase changes are important and cannot be neglected, for modeling purposes.

The particulate streams are characterized by the median diameter. The final median diameter, which is dependent on the rate of urea deposition and the average residence time of the solids, influences the hydrodynamics of the bed as well as the mass transfer between phases. Even though the size grade numbers are satisfactorily predicted, the use of average diameters is an approximation that should be removed to estimate the product particle size distribution, which has direct influence on the recycle ratios and stability of the granulation circuits. A population balance equation to estimate the outlet particle size distributions for the continuous multiple bed urea granulator is currently being implemented.

Acknowledgment

Authors express their gratitude for the financial support by the Consejo de Investigaciones Científicas y Técnicas (CONICET), the Agencia Nacional de Promoción Científica y Tecnológica (ANPCyT), the Universidad Nacional del Sur (UNS), and the Universidad Nacional del Comahue (UNCo) of Argentina.

Nomenclature

Ar = Archimedes number; $Ar = g\rho_a(\rho_s - \rho_a)D_p^3/\mu_a^2$
A_T = total cross-sectional area (m_{bed}^2)
cp = mass heat capacity (kJ/(kg K))
$\hat{c}p$ = molar heat capacity (kJ/(kmol K))
D = diameter (m)
g = gravity acceleration (m/s^2)
h = air−particle/liquid film heat-transfer coefficient (kW/(m^2 K))
$\hat{h}$ = air−surface heat-transfer coefficient (kW/(m^2 K))
H = mass enthalpy (kJ/kg)
$\hat{H}$ = molar enthalpy (kJ/kmol)
k_{EB} = emulsion-bubble mass-transfer coefficient ($m_{dry\ air}^3/m_{bubble}^2$ s)

k_{PE} = particle-emulsion mass-transfer coefficient ($m_{dry\ air}^3/m_{particle}^2$ s)
L = fluidized bed height (m_{bed})
$\dot{m}_a$ = atomization and fluidization air mass flow rate ($kg_{dry\ air}$/s)
$\dot{m}_{EV}$ = evaporated water mass flow rate (kg_{water}/s)
$\dot{m}_L$ = melt mass flow rate ($kg_{solution\ (urea\ melt)}$/s)
$\dot{m}_S$ = solid mass flow rate (kg_{urea}/s)
M = molecular weight (kg/kmol)
N_{or} = number of orifices per unit area at the distributor
P = pressure (Pa)
P^V = water vapor pressure (Pa)
$\dot{Q}$ = heat flow (kW)
R = ideal gas constant (kJ/(kmol K))
Re = particle Reynolds number; $Re = \rho_a u D_p/\mu$
S = urea solubility ($kmol_{urea}/kmol_{solution}$)
T = temperature (K)
u = velocity (m_{bed}/s)
U = overall heat-transfer coefficient (kW/(m^2 K))
x = water content, wet basis ($kg_{water}/kg_{solution}$)
X = water content, dry basis (kg_{water}/kg_{urea})
Y = mass air humidity, dry basis ($kg_{water}/kg_{dry\ air}$); $Y = [y/(1 - y)](M_w/M_a)$
y = molar air humidity ($kmol_{water}/kmol_{humid\ air}$)
z = axial coordinate (m_{bed})

Greek Symbols

α = heat-transport parameter, eq 26
β_{EB} = mass-transport parameter, eq 5 ($m_{bubbles}/m_{bed}$)
β_{PE} = mass-transport parameter, eq 4 ($m_{particle}/m_{bed}$)
δ = bubble fraction in the fluidized bed ($m_{bubbles}^3/m_{bed}^3$)
ϵ = total bed void fraction (m_{air}^3/m_{bed}^3)
ϵ_{mf} = emulsion void fraction ($m_{air}^3/m_{emulsion}^3$)
γ = activity coefficient
λ = heat-transport parameter, eq 27 ($m_{particle}/m_{bed}$)
μ = gas viscosity (kg/(m s))
ξ = evaporation parameter
ρ = density (kg/m^3)

Subscripts

a = air
APL = air−particle/liquid interface
b = bubbles
b_0 = just above the distributor
b_r = bubbles relative to the emulsion phase
DIS = dissolution
e = emulsion phase
EV = evaporated water/evaporation
ext = external, surroundings
FUS = fusion
j = chamber number
L = urea melt
N = number of external media
mf = under minimum fluidizing conditions
MIX = mixing
p = particles
S = solid
t = terminal
T = total
U = urea
V = vapor
W = water
wall = at the wall

Superscripts

i = inlet
calc = calculated value
exp = experimental value
max = maximum
o = outlet
* = equilibrium conditions

Accents

– = axially averaged

Literature Cited

(1) Litster, J.; Ennis, B.; Liu, L. *The Science and Engineering of Granulation Processes*; Particle Technology Series; Kluwer Academic Publishers: Dordrecht, The Netherlands, 2004.

(2) Ennis, B. J. Agglomeration and Size Enlargement: Session Summary Paper. *Powder Technol.* **1996**, *88*, 203.

(3) Heinrich, S.; Henneberg, M.; Peglow, M.; Drechsler, J.; Mörl, L. Fluidized Bed Spray Granulation: Analysis of Heat and Mass Transfers and Dynamic Particle Populations. *Braz. J. Chem. Eng.* **2005**, *22* (2), 181.

(4) Adetayo, A. A. Modelling and Simulation of a Fertilizer Granulation Circuit, Ph.D. Thesis, Department of Chemical Engineering, The University of Queensland, Australia, 1993.

(5) International Fertilizer Industry Association, http://www.fertilizer.org/ifa.

(6) *Fertilizer Manual*. United Nations Industrial Development Organization (UNIDO) and International Fertilizer Development Center (IFDC); Kluwer Academic Publishers: Dordrecht, The Netherlands, 1998.

(7) Uhde Fertilizer Technology, http://www.uhde-fertilizer-technology-.com.

(8) Abberger, T. The Effect of Powder Type, Free Moisture and Deformation Behaviour of Granules on the Kinetics of Fluid-Bed Granulation. *Eur. J. Pharm. Biopharm.* **2001**, *52*, 327.

(9) Boerefijn, R.; Hounslow, M. J. Studies of Fluid Bed Granulation in an Industrial R&D Context. *Chem. Eng Sci.* **2005**, *60*, 3879.

(10) Fung, K. Y.; Ng, K. M.; Nakajima, S.; Wibowo, C. A Systematic Iterative Procedure for Determining Granulator Operating Parameters. *AIChE J.* **2006**, *52* (9), 3189.

(11) Hasltensen, M.; de Bakker, P.; Esbensen, K. H. Acoustic Chemometric Monitoring of an Industrial Granulation Production Process—A PAT Feasibility Study. *Chemom. Intell. Lab. Syst.* **2006**, *84*, 88.

(12) Nijsten, P. J. B.; Starmans, P. J. M. Process for Producing Granules. U.S. Patent 5,779,945, 1998.

(13) Niks, A.; Van Hijfte, W. H. P.; Goethals, R. A. J. Process for Urea Granulation. U.S. Patent 5,653,781, 1997.

(14) Heinrich, S.; Mörl, L. Fluidized Bed Spray Granulation—A New Model for the Description of Particle Wetting and of Temperature and Concentration Distributions. *Chem. Eng. Process.* **1999**, *38*, 635.

(15) Heinrich, S.; Blumschein, J.; Henneberg, M.; Ihlow, M.; Peglow, M.; Mörl, L. Study of Dynamic Multi-dimensional Temperature and Concentration Distributions in Liquid-sprayed Fluidized Beds. *Chem. Eng. Sci.* **2003**, *58*, 5135.

(16) Ronsse, F.; Pieters, J. G.; Dewettinck, K. Combined Population Balance and Thermodynamic Modelling of the Batch Top-Spray Fluidised Bed Coating Process. Part I-Model Development and Validation. *J. Food Eng.* **2007**, *78*, 296.

(17) Jacob, M. Granulation Equipment (Chapter 9). In *Handbook of Powder Technology;* Elsevier: Amsterdam, The Netherlands, 2007.

(18) Toomey, R. D.; Johnstone, H. F. Gaseous Fluidization of Solid Particles. *Chem. Eng. Progress.* **1952**, *48*, 220.

(19) Geldart, D. Types of Gas Fluidization. *Powder Technol.* **1973**, *7*, 285.

(20) Yates, J. G. *Fundamentals of Fluidized-bed Chemical Processes*; Monographs in Chemical Engineering; Butterworths: London, 1983.

(21) Fitzgerald, T. J. Chapter 12. In *Fluidization*; Davidson, J. F., Clift, R., Harrison, D., Eds.; Academic Press: New York, 1985.

(22) Kunii, D.; Levenspiel, O. *Fluidization Engineering*; Butterworth−Heinemann: Boston, 1991.

(23) Mörl, L.; Heinrich, S.; Peglow, M. M. Fluidized Bed Spray Granulation. Chapter 2 in *Handbook of Powder Technology;* Elsevier: Amsterdam, The Netherlands, 2007.

(24) Chitester, D. C.; Kornosky, R. M.; Fan, L.-S.; Danko, J. P. Characteristics of fluidization at high pressure. *Chem. Eng Sci.* **1984**, *39*, 253.

(25) Mori, S.; Wen, C. Y. Estimation of Bubble Diameter in Gaseous Fluidized Beds. *AIChE J.* **1975**, *21*, 109.

(26) Smith, J. M.; Van Ness, H. C.; Abbott, M. M. *Introduction to Chemical Engineering Thermodynamics*; McGraw−Hill: New York, 1996.

(27) Kayaert, A. F.; Antonus, R. A. C. Process for the Production of Urea Granules. U.S. Patent 5,653,781, 1997.

(28) Botterill, J. S. M. *Fluid-Bed Heat Transfer*: Academic Press: London, 1975.

(29) Ihlow, M.; Heinrich, S.; Henneberg, M.; Peglow, M.; Mörl, L. The Problems Encountered when Calculating the Surface in Fluidized Beds Sprayed with Liquid. *Chem. Eng. Technol.* **2001**, *24*, 897.

(30) Mazza, G. D.; Mariani, N. J.; Barreto, G. F. Evaluation of Overall Heat Transfer Rates between Bubbling Fluidized Beds and Immersed Surfaces. *Chem. Eng. Commun.* **1997**, *162*, 125.

(31) Mazza, G. D.; Barreto, G. F. The Gas Contribution to Heat Transfer Between Fluidized Beds of Large Particles and Immersed Surfaces. *Int. J. Heat Mass Transfer* **1988**, *31*, 603.

(32) Incropera, F. P.; DeWitt, D. P. *Fundamentals of Heat and Mass Transfer*; Wiley: Singapore, 1981.

(33) Daubert, T. E.; Danner, R. P. *Thermodynamics Properties of Pure Chemicals: Data Compilation*; Taylor & Francis: London, 1996.

(34) *Kirk−Othmer Encyclopedia of Chemical Technology*; Wiley: New York, 1991.

Received for review March 9, 2007
Revised manuscript received June 8, 2007
Accepted June 8, 2007

IE070361O